



# UV-Curable Polyurethane-Based, Halogen-Free, $\text{CaB}_4\text{O}_7$ Nanoparticles Decorated, Flexible Flame-Retardant Films

Aslı Beyler Cigil<sup>1,2</sup> · Yusuf Samet Aytekin<sup>2</sup> · Özde Ceren Hızal<sup>2</sup> · Ayşen Yılmaz<sup>2,3</sup> · Okan Esenturk<sup>2,3,4</sup>

Received: 3 March 2025 / Accepted: 23 April 2025  
© The Author(s) 2025

## Abstract

In this study, combinations of phosphorous silicone methacrylate monomer (PSiMA) and  $\text{CaB}_4\text{O}_7$  nanoparticles (CBO NPs) were prepared for formation of halogen-free, flame-retardant, UV-curable polyurethane acrylate (PUA) films. The addition of either PSiMA or CBO NPs to PUA increased the flame-retardancy as expected, but the PSiMA-only addition, unfortunately, had adverse effects on the physical properties. However, the combined addition of PSiMA and CBO NPs not only resulted in the best performance on flame retardancy but also recovered the polymer's thermal and physical properties. With additives high initial decomposition temperatures were observed in the range of 175–216 °C. Among the combinations, PLU-60PSi-10NP (60 phr PSiMA+10 phr CBO NPs) resulted in the best LOI performance of 27, which is 40% more than the PLU film (PUA-based film). In addition, the film had a remarkable char formation ability of 14.5% compared to PLU. The observed high LOI values could not be explained by the high percentages of P, Si, B, and N in the films, but the synergy among the additives was also considered. In this study, we have investigated the use of a promising technique, THz spectroscopy, on the characterization of these films as well. Very interestingly, the results showed a nice correlation between the dielectric responses measured by THz spectroscopy and the mechanical properties of the films. Observed great performances along with the simple preparation methods of these newly developed *halogen-free, flame-retardant, PUA-based* films are expected to significantly increase their potential use in many practical applications such as automobile, leather, printing, and coatings.

**Keywords** Flexible polyurethane film · UV-curable · Halogen-free flame retardant · Calcium borate nanoparticles

## 1 Introduction

Natural and synthetic polymers are very commonly used materials in many applications such as coating, membranes, cables, sensors, electronics, etc. with their advantages

properties of low density, resistance to abrasion, and ease of processing [1–3]. However, the flammability of these polymeric materials unfortunately limits their use in many of the areas. It is important to improve the flame-retardant properties of the polymeric films, especially for a highly used polymer; polyurethane. Generally, there are two different ways for such improvement. The first method is direct addition of flame-retardant additives to the polymer matrix through melt processing or mixing. In this case, poor compatibility may occur, and it becomes difficult to form a homogeneous, stable coating solution. This generally results in poor performances [4, 5]. The second method is chemically bonding the flame-retardants to the polymer chain [6]. The chemical bonding of the flame-retardant to a polymer chain, in general, shows higher thermal stability compared to the physical addition. In addition, there is no migration of the flame-retardant in the coating over time [7]. One possible disadvantage is reduction of mechanical properties caused by incompatibility of flame-retardants with the polymer [8].

✉ Aslı Beyler Cigil  
asli.beyler@gazi.edu.tr

✉ Okan Esenturk  
eokan@metu.edu.tr

<sup>1</sup> Department of Chemistry and Chemical Process Technology, Gazi University, 06374 Ankara, Turkey

<sup>2</sup> Department of Chemistry, Middle East Technical University, 06800 Ankara, Turkey

<sup>3</sup> Department of Micro and Nano Technology, Middle East Technical University, 06800 Ankara, Turkey

<sup>4</sup> UNAM-Institute of Materials Science and Nanotechnology, 06800 Ankara, Turkey

Halogen-based flame-retardants are common and highly used example of the second method in the polymeric coatings. However, halogen-based flame-retardants produce large amounts of toxic gases during the combustion process. These gases are very harmful both to humans and the nature. *Halogen-free* flame-retardants, on the other hand, are attracting more attention recently since they do produce much fewer toxic gases and fumes during combustion [9]. Therefore, in order to protect the environment halogen-based flame retardants have been gradually replaced by green flame-retardants containing elements such as silicone [10], phosphorus [11], nitrogen [12] and boron [13, 14]. In particular, phosphorus-containing flame retardants such as phosphine oxides, phosphonates, phosphonium, phosphates, and phosphites have been extensively studied as promising alternatives for halogenated compounds [1, 15].

Phosphorus containing flame-retardants show flame-retardant effects in both condensed and gaseous phases. Decomposition of phosphorus in flame retardant systems can produce polyphosphate and phosphoric acid, which can cause dehydration of the system while catalyzing formation of carbonized layers and reactive free radicals [16]. On the other hand, nitrogen-containing flame-retardants have similar effect and decompose to produce non-combustible gases such as water, CO<sub>2</sub> and ammonia, and this way dilute the concentration of flammable gases and oxygen. Silicone containing ones are also highly efficient and preferred as green choice and works as condensed phase flame-retardant [17, 18]. In the combustion process, the formed silicate layer has a catalytic effect on formation of compact carbon layer. This way it produces an isolation and reduces the energy exchange between the combustibles and environment [19, 20]. Another preferred green choice is the boron containing flame-retardants. Here, boron forms of a glassy molten coating on the polymer surface to insulate heat and air during thermal cracking process [21, 22]. Each of these elements brings different advantages to the flame retardancy of a polymeric material and the choice of element(s) should be considered carefully based on synergy between the flame-retardants and the final composition of the polymer.

The final composition of a polymeric material is generally determined by its required properties for the application as well as its polymerization process and safety concerns. Recently, photopolymers are highly preferred materials based on their high-performance properties with ease of polymerization techniques. Photopolymerization is a process that happens by absorbing photon energy and forming active radicals called photo-initiators that initiate polymerization between monomers, reactive diluents, and oligomers in the system have advantaged over [23–25]. Diluents or solvents used in conventional coating methods often release high amounts of volatile organic compounds (VOCs) during

the preparation or use and cause great harm to human health and the environment [26, 27]. Compared to traditional coating methods, the advantages of photopolymerization can be stated with its 5Es: Environmentally friendly (low or no VOC emission), Efficient processing, Effective, Energy efficient, and Economical [28]. The solvent-free processing, faster synthesis time, and a chance to be applied at room temperature is making this a very attractive solution when applicable. In fact, in the presence of a photo-initiator, formulations in the UV curable system can be converted into a solid film or coating under UV irradiation in as little as three minutes [29].

Polyurethanes constitute a significant class of polymers widely employed in applications such as transparent and flexible coatings, hybrid systems, adhesives, synthetic leather, and numerous industrial fields due to their advantageous features including low toxicity, resistance to wear, and superior mechanical, chemical, and thermal stability [30, 31]. Among many, polyurethane acrylate (PUA) is one of the most widely used oligomers in photopolymerization. PUA combines the excellent mechanical properties of polyurethane (PU) and the superior properties of polyacrylates (PA) such as weather resistance, water resistance, and solvent resistance [32–34]. PUA is mostly used in automobile, leather, printing, and ink coatings [35, 36]. However, its flammable nature limits its use in wider application areas. Therefore, extensive efforts have been made to improve the flame-retardant properties of PUs by using various fillers including mineral fillers such as aluminum trihydroxide [34, 37, 38]. Boron compounds also reported in literature where it is directly used or used in combination with different flame-retardant additives in many polymers, including polyurethanes, provided flame-retardant benefits in the condensed phase and gas phases [39–42].

A UV-curable, non-flammable, polyurethane acrylate-based coating containing boron nanoparticles, thus, appears to be a very promising alternative as a flame-retardant material carrying all the attractive PU properties. In spite of their promising attributes, only two studies in the literature were found on boron containing PUA composites and none have investigated the flame retardancy. In a study by Kim et al. [43], UV curable boron nitride (BN)/PUA composite was prepared to obtain undersea sonar encapsulator through surface modifications. It was mentioned that better dispersibility and stronger interaction were provided on the surface and was concluded that these composites were promising materials as sonar encapsulators and could significantly increase both mechanical strength and long-term stability. In a study by Liu et al. [13], a series of water-based polyurethanes (WPU) were prepared using an end-capping agent, diallylamine (glycidoxypropyl)methyldiethoxysilane (DAA-GPTMS) and hydroxylated boron nitride (hBN-OH)

nanolayers. As a result of wettability experiments and water absorption tests, it was stated that the addition of DAA-GPTMS significantly improved the hydrophobicity and water resistance of WPU films. In addition, it was emphasized that a synergistic effect was obtained between DAA-GPTMS and hBN-OH, thus improving the mechanical and physical properties of the films. Considering the significant uses of polyurethane-based polymers in many application areas, there is a need to increase the flame retardancy without sacrificing its mechanical and thermal properties. Such studies will enable to develop PUA composites with better performances and will attract the interest of the scientific community and also of the industrial partners.

There are many commonly used characterization techniques for determining the properties of polymeric materials. Terahertz (THz) spectroscopy is becoming a developing tool for analysis of polymeric materials, too. THz region of the electromagnetic spectrum is located in between microwave and infrared regions, and generally referred as 0.1–10 THz frequency band. With its long wavelengths THz beams can penetrate through most dielectric materials such as ceramics, glass, polymers, and rubber while metals do not transmit the THz signal. With its unique properties, THz spectroscopy has been broadly used in many areas like material sciences [44, 45], chemistry [46], engineering [47], biology [48] and security applications [49]. THz techniques in general are non-destructive testing methods for characterization of polymeric materials as such polymers containing nanocomposites for their homogeneity and dispersion [50–52], polymeric thin films [53, 54] for their dielectric response, inspection for laminate properties of polymers [55], etc. In this study we would also like to investigate the possible use of THz spectroscopy as a complementary technique for the characterization of the newly prepared polyurethane-based nanoparticle decorated flame-retardant films.

The need to enhance the flame retardancy of polyurethane-based polymers without compromising their mechanical and thermal properties is a notable concern across the academia and various industries. Therefore, in this study a monomer containing phosphorus, silicone, and acrylate groups was synthesized and UV curable films were prepared by mixing polyurethane acrylate PSiMA oligomer and calcium tetraborate nanoparticles (CBO NPs) at determined combination amounts. The PSiMA monomer was characterized using FTIR spectroscopy. The synergistic effect of phosphorus, silicone, boron, and nitrogen contributing to the flame-retardancy were investigated by comparing the limiting oxygen index (LOI) values. In addition, we have characterized the optical properties of the PLU film and its composites using a new technology, THz-TDS. The mechanical, thermal, and surface properties of all films were

also characterized and compared and effect of PSiMA and nanoparticles on these properties were discussed.

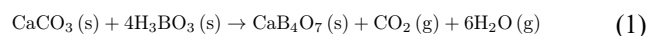
## 2 Experimental

### 2.1 Materials

Aliphatic polyester-based urethane diacrylate oligomer blended with 25% ethoxylated trimethylol propane triacrylate. (AUA; CN963E75) was purchased from Sartomer (Verneuil en Halatte, France). 1-vinyl-2-pyrrolidone (NVP), diethylphosphonoacetic acid (DEPA), glycidyl methacrylate (GMA), 3-(trimethoxysilyl)propyl methacrylate (MEMO) and phenylbis(2,4,6-trimethyl benzoyl) phosphine oxide (Irgacure 2022) were obtained from Sigma Aldrich. P-toluenesulfonic acid (p-TSA) was purchased from Ataman Kimya (Turkey).  $\text{CaCO}_3$  (98% purity) and  $\text{H}_3\text{BO}_3$  (99.5% purity) were purchased from Merck.

### 2.2 Synthesis of the $\text{CaB}_4\text{O}_7$ Nanoparticles

$\text{CaB}_4\text{O}_7$  nanoparticles (CBO NPs) were produced via solid-state synthesis method. Stoichiometric amounts of  $\text{CaCO}_3$  and  $\text{H}_3\text{BO}_3$  were ground thoroughly in an agate mortar for homogeneity. Then the mixture was calcinated in the muffle furnace attuned to heat up at 850 °C with a 4 °C/min heating rate, and retention time was adjusted to 2 h at this temperature.



### 2.3 Synthesis of Phosphorous Silicone Methacrylate (PSiMA) Monomer

To prepare phosphorus silicone methacrylate (PSiMA) monomer, diethylphosphonoacetic acid (1.96 g) and glycidyl methacrylate (1.42 g) were added into a 100 mL three-necked flask equipped with a magnetic stirrer and a condenser. The mixture was stirred in a nitrogen atmosphere. After the temperature was increased to 60 °C, p-toluenesulfonic acid (p-TSA) (1 wt %) was added as a catalyst, and the reaction was continued for 3 h. hydMEMO was prepared similar to previous studies in the literature [56]. Briefly, hydMEMO was obtained by mixing MEMO, ethanol, distilled water, and catalyst (p-TSA) (0.05 wt%) at room temperature for 12 h. Then, the temperature was reduced to 40 °C, and hydrolyzed 3-(trimethoxysilyl)propyl methacrylate (hydMEMO) (7.44 g) was added. The reaction was continued for 1 h, and PSiMA monomer was obtained as a transparent yellow liquid. The synthesis routes are given in Fig. 1.

**Fig. 1** Synthesis of phosphorous silicone methacrylate (PSiMA) monomer

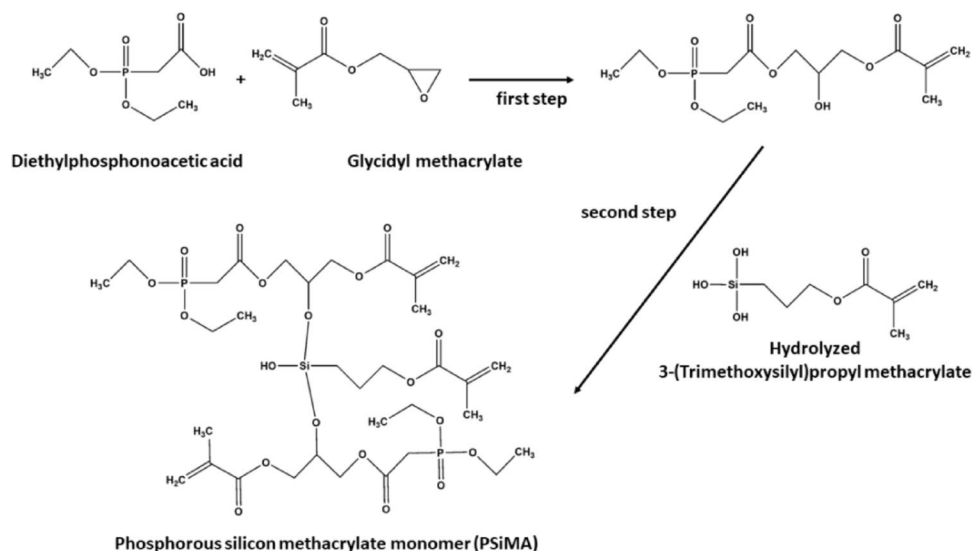


**Table 1** Formulations of UV-curable films

Code	AUA (wt%)	NVP (wt%)	PSiMA (phr)	CBO NPs (phr)
PLU	80	20	-	-
PLU-5 NP	80	20	-	5
PLU-10 NP	80	20	-	10
PLU-20PSi	80	20	20	-
PLU-20PSi-5 NP	80	20	20	5
PLU-20PSi-10 NP	80	20	20	10
PLU-40PSi	80	20	40	-
PLU-40PSi-5 NP	80	20	40	5
PLU-40PSi-10 NP	80	20	40	10
PLU-60PSi	80	20	60	-
PLU-60PSi-5 NP	80	20	60	5
PLU-60PSi-10 NP	80	20	60	10

## 2.4 Preparation of the UV-Curable Films

The UV-curable films solution consisted of aliphatic urethane acrylate prepolymer (AUA), PSiMA monomer, calcium tetraborate nanoparticles, 1-vinyl-2-pyrrolidone (NVP), and photo-initiator (P-I, Irgacure 2022). The materials listed above (excluding the P-I) were mixed in a 50 mL beaker according to the amounts given in Table 1 and kept in an ultrasonic bath for 30 min until a homogeneous solution was obtained. According to the change in the amount of PSiMA monomer and calcium tetraborate nanoparticles (CBO NPs) in the formulations, 12 different formulations were prepared. The bubbles formed in the prepared formulations were removed by keeping them in an oven at 40 °C, then the mixture was cooled to room temperature and P-I was added. The mixtures were then poured into Teflon® molds and cured for three minutes under UV irradiation (OSRAM, 300 W,  $\lambda_{\max} = 365$  nm, 10 mW/cm<sup>2</sup>). The preparation of UV-curable films is shown in Fig. 2.

## 2.5 Characterization

Fourier Transform Infrared Spectroscopy (FTIR) spectra were recorded on a Thermo Nicolet iS10 spectrometer in the range of 4000–600 cm<sup>-1</sup> to explain the structures of DEPA, GMA, hydMEMO, PSiMA monomer, and UV-curable films. Thermal gravimetric analyzes (TGA) of the UV-curable films were performed by using a Perkin Elmer Instrument STA6000. Samples were run from 30 to 750 °C with a heating rate of 10 °C/min under a nitrogen atmosphere. The structural parameters of the synthesized NPs were determined with X-Ray Diffraction (XRD) technique using Rigaku Miniflex X-Ray Diffractometer with CuK $\alpha$  source (30 kV, 15 mA,  $\lambda$  1/4 1.54051 Å) at 2 $\theta$  angles from 5° to 90° at 1°/min rate. Limiting oxygen index (LOI) values of the UV-curable films were measured according to ASTM D2863-08. For each sample, at least three measurements were made, and the average was reported with an accuracy of  $\pm 0.8$ .

The morphology of the UV-curable films was examined with a Carl-Zeiss Evo40 scanning electron microscope

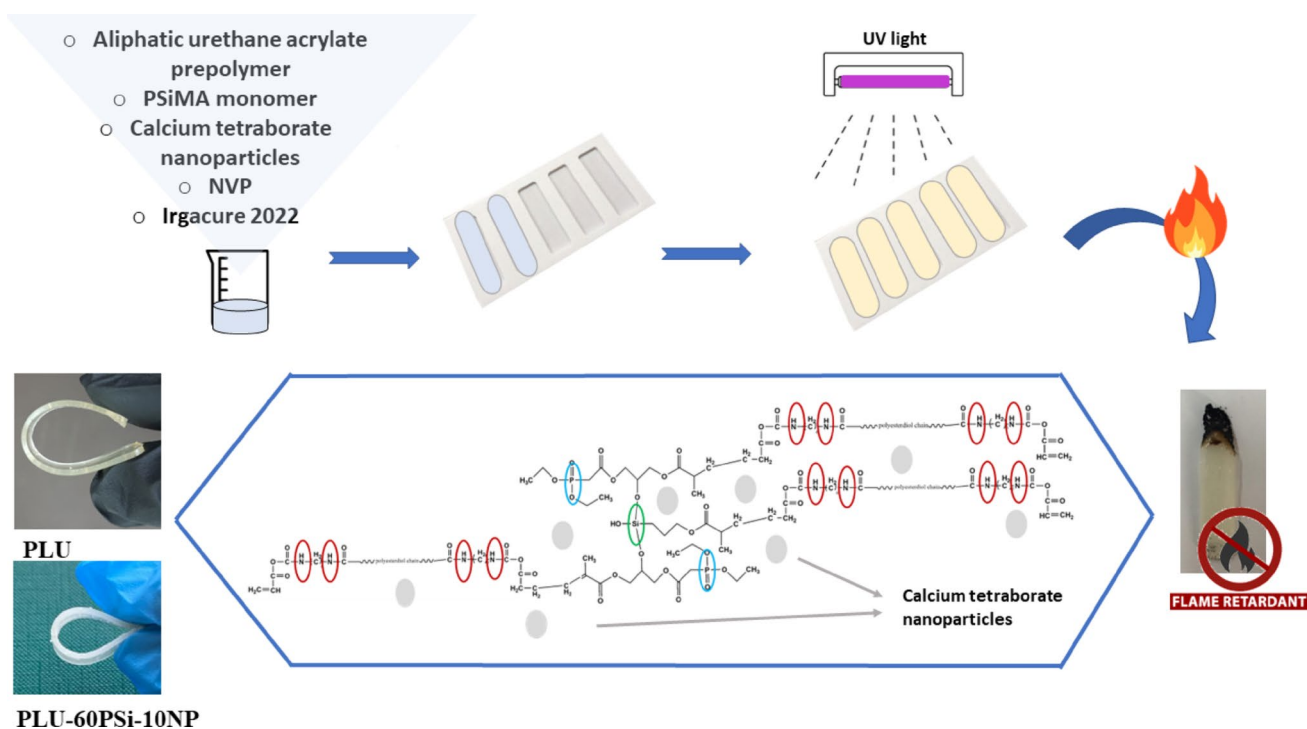


Fig. 2 Preparation of UV-curable films

(SEM). The films were first broken, then sputter-coated with a 20 nm layer of gold/palladium on the surface to improve conductivity and prevent charging prior to investigation. The water contact angles (WCAs) of the UV-curable films were determined at room temperature on an Attension Theta Lite optical tensiometer. Measurements were made using 3–5  $\mu\text{L}$  drops of distilled water. For each film, at least five measurements were made, and the average was taken. The drop images were processed with an image analysis system, which calculated both the right and left WCAs from the shape of the drop with an accuracy of  $\pm 0.6^\circ$ . The mechanical properties of the UV-curable films were determined at room temperature with a Materials Tester Z010/TN2S. Shore A scale hardness of UV-curable films were carried out by Loyka LX-A-1. For each film, at least five measurements were made, and the average was reported with an accuracy of  $\pm 0.5$ .

Terahertz Time-Domain Spectroscopy (THz-TDS) is also utilised for probing the dielectric changes upon addition of both PSiMA monomer and  $\text{CaB}_4\text{O}_7$  nanoparticles. The transmitted THz signal through the films was analysed in the range of 0.18–1.5 THz by extracting static properties namely absorption coefficient and refractive index. The details of the THz time domain spectrometer is described elsewhere [57]. To briefly mention, an oscillator Ti: Sapphire laser having 80 fs pulse duration, central wavelength of 800 nm, and frequency of 80 MHz is used as the light source. The output beam of the laser is split into two for

pumping the GaAs antenna for THz light production and for indirect detection of THz light by using birefringent ZnTe crystal with  $\langle 110 \rangle$  orientation with electrooptic sampling. The effective bandwidth relies on the transmission properties of the sample lying in 0.1–1.5 THz range for the obtained polymeric film samples for this work. THz light path is purged with dry air to eliminate light attenuation by humid air and all measurements were done in this purged chamber. The sample UV-curable films were measured at 21  $^\circ\text{C}$  and less than 1% humidity.

### 3 Results and Discussion

#### 3.1 Structural Characterization of $\text{CaB}_4\text{O}_7$ Nanoparticles

Figure 3 presents the XRD pattern of the synthesized  $\text{CaB}_4\text{O}_7$  nanoparticle (CBO NPs). The peaks in the XRD pattern match well with the JCPDS card no. 31-0253 of  $\text{CaB}_4\text{O}_7$ , crystallized in a monoclinic structure with a space group of  $P21/n$  (space group no. 14) and with unit cell parameters of  $a = 12.264 \text{ \AA}$ ,  $b = 9.895 \text{ \AA}$ ,  $c = 7.796 \text{ \AA}$ . All the significant peaks of the pattern were identified and labeled according to the Miller indices (hkl). The agreement of XRD patterns with the card indicates that calcium tetraborate structures were successfully obtained. Furthermore, the sharpness and intensity of the peaks indicate good crystallinity of the

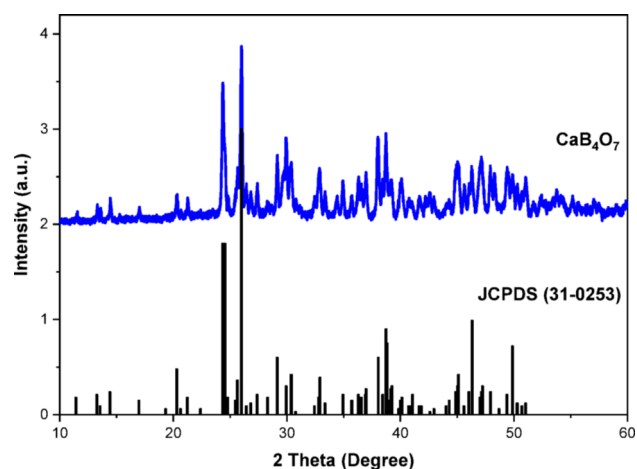


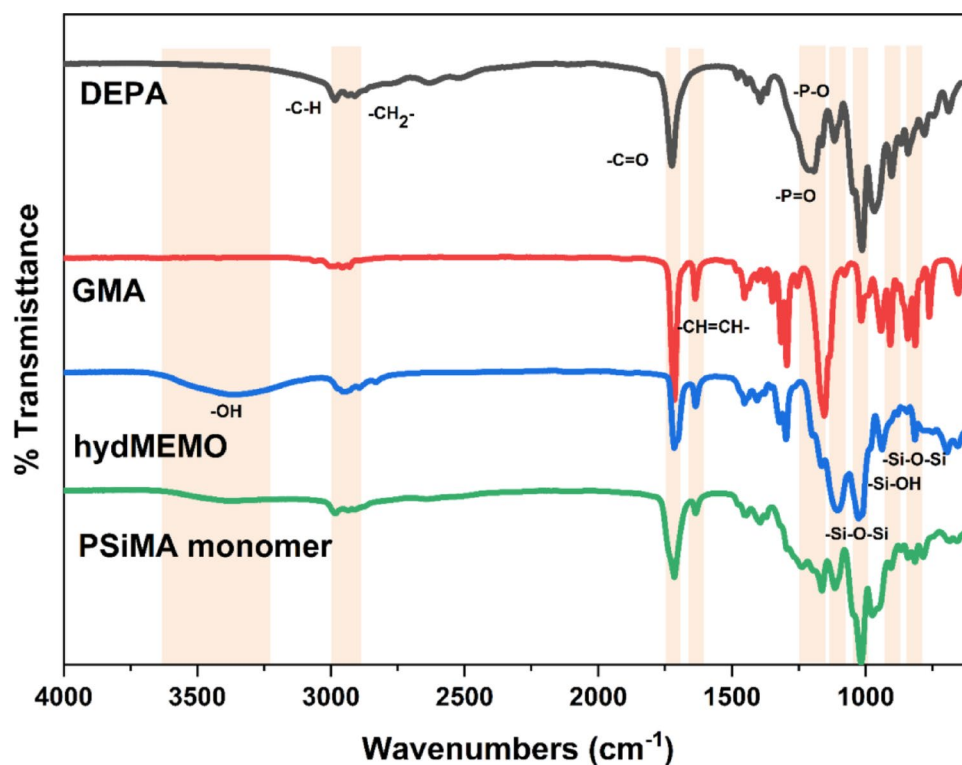
**Fig. 3** XRD pattern of  $\text{CaB}_4\text{O}_7$  nanoparticles (CBO NPs)

sample, suggesting that the reaction proceeded efficiently under the conditions described. This confirms the purity of the phase and the absence of secondary products.

### 3.2 Structural Characterization of Phosphorous Silicone Methacrylate Monomer

In this study, we synthesized a halogen-free monomer that can reduce the flammability of UV-curable films. Phosphorous silicone methacrylate (PSiMA) monomer was synthesized from the reaction of DEPA, GMA, and hydMEMO. The chemical structures of DEPA, GMA, hydMEMO, and PSiMA monomer were characterized by FTIR, and the

**Fig. 4** FTIR spectra of DEPA, GMA, hydMEMO, and PSiMA monomer



corresponding FTIR spectra are shown in Fig. 4. In the FTIR spectra of the PSiMA monomer, a strong band at  $1720\text{ cm}^{-1}$  is due to carbonyl group stretching vibrations of DEPA, GMA, and hydMEMO while the band at  $1162\text{ cm}^{-1}$  is due to the ether group stretching vibrations of DEPA, GMA, and hydMEMO. The asymmetric stretching vibrations of the C-H bonds in the methyl and methylene groups of DEPA, GMA, and hydMEMO are seen at  $2932$ , and  $2845\text{ cm}^{-1}$ , respectively [58–60]. Additionally, the characteristic peaks at  $1230\text{ cm}^{-1}$ , and  $1052\text{ cm}^{-1}$  were attributed to the P-O-C, and P=O groups of DEPA, respectively. The Si-O-Si group peaks of hydMEMO at around  $1019\text{ cm}^{-1}$ ,  $1091\text{ cm}^{-1}$ , and  $814\text{ cm}^{-1}$  are also present in these spectra. The fact that the peak belonging to the symmetric stretching vibration of the epoxy groups at  $910\text{ cm}^{-1}$  in the GMA spectrum [61] which is not seen in PSiMA monomer indicates that the ring-opening reaction with the carboxylic acid in DEPA has taken place. In addition, a small absorption peak at  $1637\text{ cm}^{-1}$  shows the carbon-carbon double bonds of the acrylate groups of PSiMA monomer [62]. All these results indicated that the phosphorous silicone methacrylate (PSiMA) monomer was successfully synthesized.

### 3.3 Structural Characterization of the UV-Curable Films

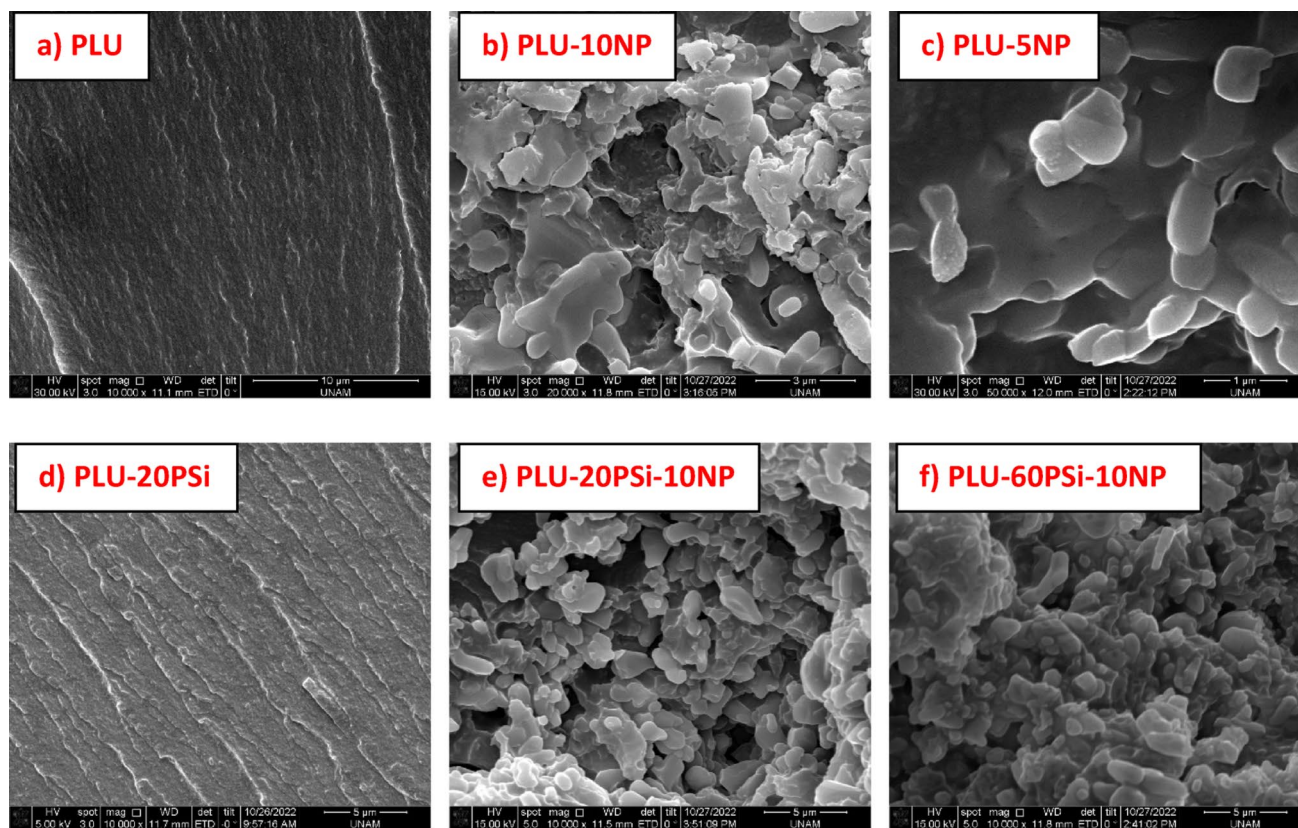
The characteristic absorption bands for a series of UV-curable films prepared with polyurethane acrylate oligomers were observed at  $1710\text{ cm}^{-1}$  (C=O),  $1540$  and  $3340$

$\text{cm}^{-1}$  (N–H),  $2960 \text{ cm}^{-1}$  ( $-\text{CH}_3$ ), and  $1100 \text{ cm}^{-1}$  (C–O–C) in the FTIR spectra (see Supp. Figure 1). The spectra were compatible with UV-curable films prepared with urethane acrylate in the literature [63]. With the PSiMA monomer inclusion, new absorption bands were observed at  $1230 \text{ cm}^{-1}$ ,  $925 \text{ cm}^{-1}$  and  $1019 \text{ cm}^{-1}$  for the vibrations of P=O, P–O and Si–O, respectively. This demonstrates the successful incorporation of PSiMA monomer into polyurethane-based films. In addition to all these, addition of CBO NPs to the polymer resulted in a strong band at  $1420 \text{ cm}^{-1}$  and a shoulder  $1470 \text{ cm}^{-1}$  corresponding to the stretching mode of B–O bonds [64]. The acrylate group absorption band at  $1635 \text{ cm}^{-1}$  were completely disappeared as an evident for the UV cured film formation (See Supp. Figure 1).

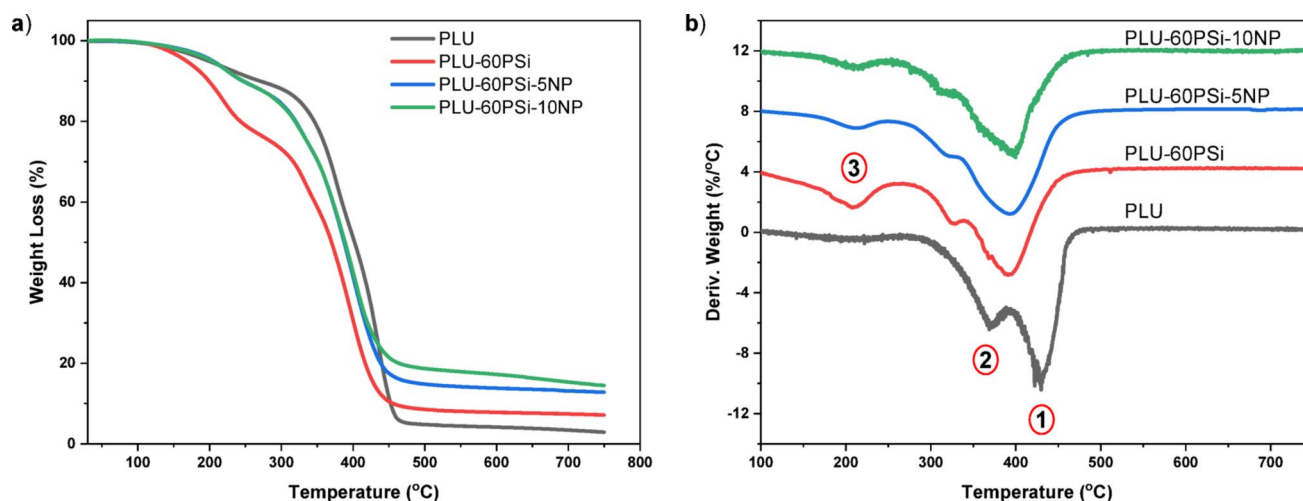
### 3.4 Surface Morphology of the UV-Curable Films

Scanning electron microscopy (SEM) images of the PLU, PLU-5 NP, PLU-10 NP, PLU-20PSi, PLU-20PSi-10 NP, and PLU-60PSi-10 NP films are given in Fig. 5. All the films exhibited uniform surfaces and no significant aggregation was observed when either PSiMA or NPs or both were added to the PLU. The PLU film (Fig. 5a) and the others (i.e. Fig. 5d) had plain and smooth surface morphology. The aliphatic urethane acrylate/CBO nanocomposite films with

5 and 10 parts per hundred (phr) NPs (PLU-5 NP and PLU-10 NP), had similar homogenous surfaces as the control film (PLU) and their fractured surface images (Fig. 5b and c) showed well-dispersed CBO nanoparticles in the AUA and NVP matrix. They are given in two different magnifications as example representations of the film structures. The film containing 60 phr PSiMA and 10 phr CBO NPs (PLU-60PSi-10 NP) with the highest content of phosphorus, silicon, and nanoparticles also exhibited a homogenous surface. It appears that PSiMA homogeneously dispersed even in PLU-60PSi, PLU-60PSi-5 NP, or PLU-60PSi-10 NP (Fig. 5f) formulations that are containing 60 phr PSiMA monomer at the greatest amount. Evaluation of the formulations with 10 phr NPs (PLU-20PSi-10 NP, PLU-40PSi-10 NP, and PLU-60PSi-10 NP) revealed that there were no significant aggregation problem and that the nanoparticles were also uniformly dispersed in general in the polymer matrix. The results shows that the synergic interactions of the PLU, PSiMA and NPs formed a uniform, well dispersed films.









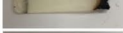


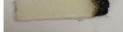


**Fig. 5** SEM images of surfaces (a and d) and fractured (b, c, d, and f) UV-curable films at various magnifications as examples of the samples' morphology



**Fig. 6** a) TGA thermograms and b) their derivatives of the PLU, PLU-60PSi, PLU-60PSi-5NP, and PLU-60PSi-10NP

**Table 2** Thermal properties of the UV-curable films

Code	$T_{\max}^1$ (°C)	$T_{\max}^2$ (°C)	$T_{\max}^3$ (°C)	Char (%)	LOI	Image
PLU	-	341.9	413.7	2.9	19.5	
PLU-5NP	-	346.3	415	6.4	23.3	
PLU-10NP	-	346.4	416.2	7.3	24.8	
PLU-20PSi	174.8	309.5	377.3	7.1	22.1	
PLU-20PSi-5NP	215.9	346.11	416.1	6.9	22.8	
PLU-20PSi-10NP	181.7	340.1	410.2	8.5	25.2	
PLU-40PSi	182.9	317.6	369.7	7.9	23.7	
PLU-40PSi-5NP	183.1	318.3	371.4	10.6	23.8	
PLU-40PSi-10NP	198.4	330.2	398.4	10.9	26.3	
PLU-60PSi	185.7	312.2	365.5	7.2	23.9	
PLU-60PSi-5NP	198.3	330.7	402.6	12.8	24.5	
PLU-60PSi-10NP	198.9	330.9	403.5	14.5	27.2	

$T_{\max}^1$ ,  $T_{\max}^2$  and  $T_{\max}^3$  are the maximum weight loss temperatures, which were determined from the maximum of the corresponding derivative curves

### 3.5 Thermal and Flame-Retardancy Properties of the UV-Curable Films

The thermal properties of the UV-curable films were determined using TGA. TGA thermograms and derivatives (DTG) of PLU, PLU-20PSi, PLU-20PSi-5 NP, and PLU-20PSi-10 NP films are shown in Fig. 6a and b as a representation of all the compositions. (TGA thermograms of all films are presented in Supp. Figure 2). The maximum weight

loss temperatures (determined from the maximums of the corresponding derivative curves) and the char yields at 750 °C are given in Table 2. In general, the thermal decomposition of polyurethane under nitrogen atmosphere consisted of two stages, marked as 1 and 2 in the Fig. 6b. First one originated from the hard segment carbamate and the second one originated from the soft segment polyether contained in the polyurethane acrylate. After the addition of 5 phr and 10 phr CBO NPs (PLU-5 NP and PLU-10 NP, respectively)

the maximum degradation temperature was increased very slightly (Table 2). Meantime, a significant increase in char was observed with NPs addition as expected. The results show that the NPs do mix well with the PLU and does not change the thermal characters of the films significantly. However, the addition of the flame-retardant monomer (PSiMA) to the polyurethane acrylate (PLU-xPSi; x = 20, 40, 60), mixture film thermal decomposition took place mainly in three stages; decomposition of the flame-retardant components, the hard segment, and the soft segment. In addition, it appears that the PLU decomposition temperatures were also shifted to lower temperatures compare to the control film (PLU).

In these films, early decomposition of the PSiMA is expected since it is well-known in the literature that phosphorus-based flame-retardants begin to degrade at a lower temperature [65–69]. This is possibly because of the weaker P-O-C bond strength in PSiMA monomer compared to the C-C bond in the polymer structure. In a similar study of another UV-curable flame-retardant containing 9,10-dihydro-9-oxa-10-phosphaphenanthrene-10-oxide (DOPO) have reported around 310 °C [69]. This agrees with the  $T_{\max}$  of our films (PLU-20PSi, PLU-40PSi and PLU-60PSi) that do not contain CBO NPs. These results show that the PSiMA or phosphorous containing flame retardants tend to lower the thermal decomposition temperature, thus adversely affect the thermal strengths of the control film, PLU. However, addition of these flame retardants does increase the char of the films, thus help on the flame resistivity of these films as stated in the introduction part.

Addition of NPs to the PSiMA containing films did benefit from the synergic effect of both flame retardants. The char yield of the films was significantly improved compared to the control film, PLU. The best performance was observed by the addition of 60 phr PSiMA and 10 phr CBO NPs to the PLU (PLU-60PSi-10 NP) where the char amount was increased from 2.9 to 14.5%. An increase in char amount inhibits the exchange of heat and oxygen with the environment [70, 71]; thereby, helping the flame retardancy. In these films, also, the decomposition of PSiMA monomer at high temperatures were expected to form non-combustible condensed phase compounds such as phosphorus oxides ( $PO_x$ ) that blocks the air supply to the surface for further combustion. In addition, NPs will also help the char formation on the burning layer that will prevent or delay the access to the flammable components as observed in the LOI and corresponding images of the films.

Relative flammabilities of UV-curable films were evaluated with LOI and the values obtained, and images of post-combustion films are given in Table 2. The results show that the flame-retardancy of films containing CBO NPs and PSiMA monomer are improved compared to the

control formulation (PLU). In a study by Beyler Çiğil [72], LOI value was reported as 24.3 for UV-curable coatings prepared with polyurethane acrylate, phenyl phosphine oxide (DAPPO) with acrylate functionality, 1 H,1 H,2 H,2Hperfluorodecyl acrylate, and POSS with acrylate functionality. It is known that fluorine helps on flame retardency. With our flame-retardant monomer and CBO NPs addition to the UV-curable PU film we have reached a higher LOI value of 27.2 without having a poisonous fluorine-containing monomer. This is a significant improvement compared to the current reported LOI [72] of a similar film. Many of our films have shown better performances and these high LOIs are not only due to the high percentages of P, Si or B in the formulations, but also due to the synergy of those units within the polymer film. This effect is also reflected in the dense char structure formed.

We need to mention that a higher LOI value of 31 was reported by Wang et al. for a composite system [68]. In their study, results of a UV-cured composite system containing acrylate functional PU oligomer, ethylene glycol methacrylate phosphate and nano-silica were reported. However, it was also reported that the thermal stability of the system decreased from 442 °C to 368 °C in a nitrogen atmosphere with increasing phosphorus and silica nanoparticle content. In our study, the thermal stability of the best UV-curable film (with the highest phosphorus and NP content) only slightly decreased from 413 °C to 403 °C in a nitrogen atmosphere, indicating that the added additives did not adversely affect the thermal stability.

### 3.6 Wettability of the UV-Curable Films

The water contact angle (WCA) values of the films were measured to evaluate the effects of PSiMA and CBO NPs addition on the wettability of the UV-curable films (Fig. 7). When the content of the NP was 0 phr (PLU), 5 phr (PLU-5 NP), and 10 phr (PLU-10 NP), the corresponding WCA increased from 59° to 67°, and finally to 72°, respectively. This increase in hydrophobicity appeared to be counter intuitive at first with the NPs addition since the NPs are hydrophilic. The reason for the observed increase was attributed to the surface roughness increase with NPs addition [73]. NPs appears to be covered with polymer and not open to water contact on the surface. Next, the WCAs of the films containing PSiMA monomer were examined. With the addition of 60 phr of PSiMA monomer contact angle significantly increased from 59° to 72°. Addition of PSiMA was expected to increase the roughness due to the migration of inorganic part to the surface. However, we did not observe a direct correlation of contact angle to the PSiMA content increase possibly due to varying amount of monomer part ending up on the surface. One should also consider that the relative

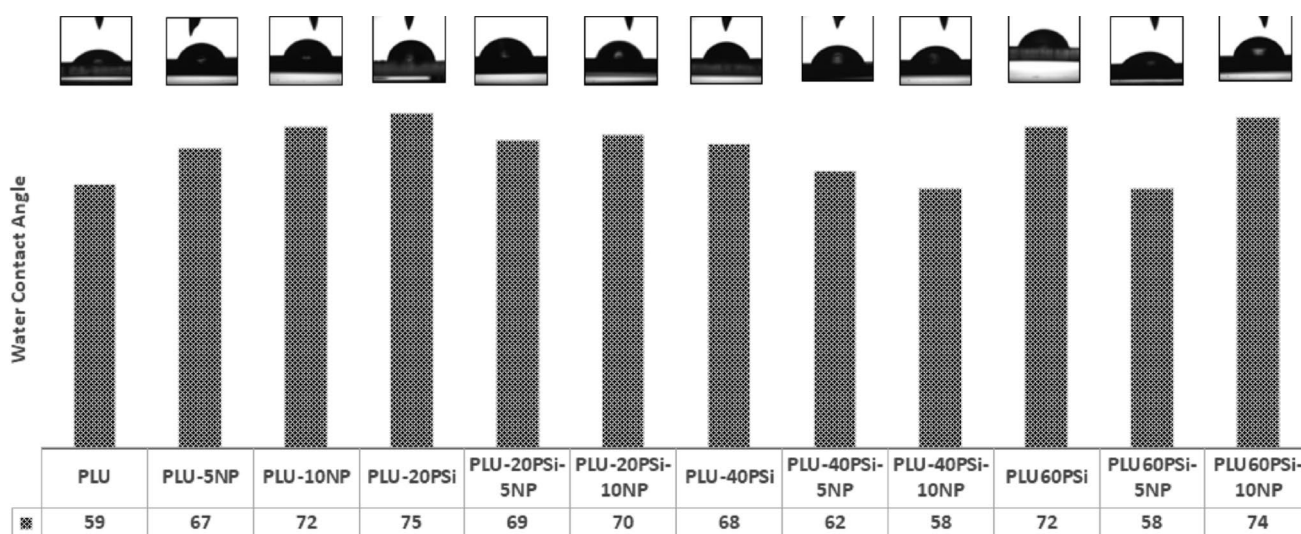
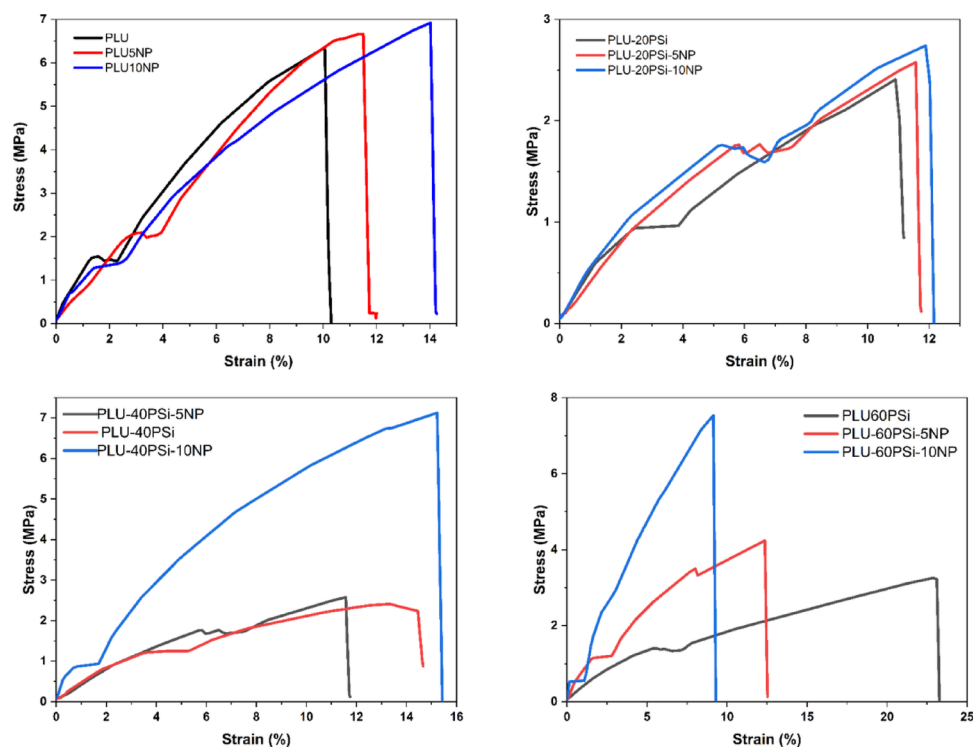


Fig. 7 WCA values of the UV-curable films

Fig. 8 Mechanical properties of UV-curable films



amount of PU chain structure decreases as the amount of PSiMA increases (i.e. the addition of 60 phr PSiMA monomer to PLU lowered the polyurethane relative amount in the film by a factor of 1.6). Therefore, when the wettability of the film with the highest PSiMA content (PLU-60PSi) was compared with that of PLU, the amount of polar urethane and urea groups on the surface of the PLU film decreases compared to PLU reference film. This caused a decrease in the surface energy of the PLU-60PSi film and contributed to the observed increase its hydrophobicity. Interestingly the contact angles of the PLU-xPSi films decreased with the

addition of the NPs, except the PLU-60PSi-10 NPs. In this case, the NPs may not have affected the surfaces as much they did in the PLU only films. On the other hand, the most hydrophobic film was PLU-60PSi-10 NPs.

### 3.7 Mechanical Properties of the UV-Curable Films

Figure 8 shows the tensile behaviors of the nanocomposite films, in which the effects of PSiMA monomer and CBO NPs on the mechanical properties of the films were observed. Table 3 shows a series of performance indices for

**Table 3** Mechanical properties of UV-curable films

Code	Young's Modulus (MPa)	Tensile Strength (MPa)	Elongation at Break (%)	Hardness (Shore A)
PLU	108.20	6.37	10.15	67
PLU-5NP	125.53	6.67	11.41	69
PLU-10NP	163.77	6.94	14.09	75
PLU-20PSi	48.58	2.41	10.92	59
PLU-20PSi-5NP	41.56	2.58	11.60	72
PLU-20PSi-10NP	57.78	2.76	12.01	74
PLU-40PSi	54.03	2.41	14.33	58
PLU-40PSi-5NP	46.31	2.57	11.75	70
PLU-40PSi-10NP	177.69	7.14	15.29	72
PLU-60PSi	35.11	3.27	23.06	58
PLU-60PSi-5NP	117.26	4.24	12.38	62
PLU-60PSi-10NP	285.71	7.54	9.15	68

UV-curable films; Young's modulus (MPa), Tensile strength (MPa), Elongation at break (%), and Hardness (Shore A). Although flame-retardant monomers outperform conventional monomers, it is a known issue in the literature that they generally have negative effects on mechanical properties [69]. In this study, some of the mechanical properties of the films were reduced when PSiMA monomer was added while the others did improve. As the PSiMA monomer content increased, the average tensile strength of the UV-curable films decreased from 6.37 MPa to 2.41 MPa. On the other hand, the increase of PSiMA monomer content to 60 phr led to a significant increase in elongation at break from 10.15 to 23.06%. It is known that increasing PSiMA monomer reduced the crosslinking density [18, 23], thus this made the films more flexible. This may also be due to the easier rotation of Si-O-Si, resulting in the higher movement/reorganization in PLU-60PSi film. In a study by Phalak et al. [1], acrylated cardanol diphenyl phosphate (ACP) was synthesized and used as a reactive diluent alongside urethane acrylate (UA) in a UV-curable system. Similar to our study, the elongation at break of UV-cured coatings increased with the addition of ACP. In the study, UV-curable coatings showed good flexibility with variation of ACP content. Similarly, the PSiMA content increased the flexibility of the UV-curable PLU films in our composite systems.

While addition of PSiMA resulted a decrease in the tensile strength, addition of the CBO NPs slightly increased the tensile strength of these UV-curable films from 6.37 to 6.94 MPa. Thus, NPs addition was expected to compensate at least some part of the loss in the strength of the UV-cured polymer due to PSiMA content. The findings for other properties were much better than compensation. As listed in Table 3, NPs addition to the PSiMA added PLU polymers served as both reinforcing fillers and cross-linking components in the composite materials. The tensile strength is not only recovered but also significantly improved with increasing CBO NPs content, especially for PLU-60PSi-10 NPs. It reached to the highest value of 7.54 while keeping

the polymer still flexible. The good compatibility of the CBO NPs with the aliphatic urethane acrylate matrix was a precondition of the nano reinforcement effect, which allows nanocomposite materials to withstand higher tensile stresses. Similar results have previously been reported in the literature with the addition of carbon nitride quantum dots to unsaturated polyester [74]. We have to note that the positive affect was lost with the use of large quantity of PSiMA (60 phr), in which the relative PLU amount decreases significantly. While the tensile strength still increased, a sharp decrease on elongation at break was observed with 10 phr NPs addition. On the other hand, we noticed that addition of the NPs to PLU increased the modulus quite significantly, which was also seen as an improvement from the strength and elongation in the Table 3. In fact, the highest recorded Young's modulus value of ca. 286 MPa was achieved with PLU-60PSi-10 NP. In addition, the hardness (Shore A) was also increased with the addition of CBO NPs. Shore A of the control film, PLU was 68. PLU-5 NP film and PLU-10 NP film were measured as 70 and 75, respectively. These effects were attributed directly to the CBO NPs, which also constrained the mobility of polymeric chains inside the aliphatic urethane acrylate nanocomposite and decreased the free volume. On the other hand, addition of monomer PSiMA, which contains phosphorus and silicone, lowered the hardness of the control film. Further additions of the monomer did not affect the hardness values. For example, the hardness of PLU-20PSi, PLU-40PSi, and PLU-60PSi was all about 60. Similarly, NPs addition to these films did increase the hardness as expected. In fact, hardness of PLU-60PSi-10 NP was 68, showing the recovery to the original value film hardness. We can say that the NPs synergy on UV-cured PLU made a better polymer at least when the mechanical properties are considered. A significant finding is that the CBO NPs mostly compensated the negative effects of PSiMA on the mechanical properties of PLU.

### 3.8 Terahertz Spectroscopy

THz spectroscopy is a diverse spectroscopic technique than can measure the dielectric properties of non-metallic systems; such as composites, polymers. The technique is especially good to observe the dielectric changes associated with the modification in the host structure. Thus, the use of THz-TDS in this study aims to evaluate the strength of THz spectroscopy for the evaluation of these fire-retardant composite systems. The THz properties of the materials were evaluated by extracting absorption coefficient and refractive indices of the UV-curable films by analyzing their transmitted THz signal measured by THz-TDS at room temperature. The system and the measurement details are given in the experimental part. A representative time domain profile and frequency domain spectra of the dry air as reference and a PLU film as sample were given in Supp. Figure 4.

The time domain data can be transferred to frequency domain by Fast Fourier Transform, by which the amplitude and the phase of the waves are decoupled, and frequency dependent absorption coefficients and refractive indices of the samples were calculated. In current measurements, the signal-to-noise (SNR) was maximized around 0.6 THz due to the transmission losses of THz waves through these PLU films. The workable bandwidth was obtained between 0.2 and 1.5 THz region. In this study we compared the absorption coefficients and indices. The frequency dependent absorption coefficients of the UV-cured films are given in Fig. 9. The absorption coefficients of the films did not change significantly with the addition of CBO NPs to the films and followed a similar trend of the host PLU films as almost linear increase up to 60  $\text{cm}^{-1}$ .

Comparing the absorption coefficients at 0.6 THz (at the highest SNR), we noticed that a slight decrease from ca. 13.3  $\text{cm}^{-1}$  of PLU to ca. 12.7  $\text{cm}^{-1}$  PLU-5 NPs was occurred and then an increase was observed to 14.5  $\text{cm}^{-1}$  with addition of 10 phr NPs (PLU-10 NPs) (Fig. 9a). Addition of 20 phr PSiMA monomer increased the coefficient to 15.9  $\text{cm}^{-1}$  but NPs addition to PLU-20PSi resulted a decrease to 15.3  $\text{cm}^{-1}$  with 5 phr and to 14.7  $\text{cm}^{-1}$  with 10 phr NPs addition (Fig. 9b). On the other hand, addition of 40 phr PSiMA monomer

to the PLU caused a further decrease in the absorption coefficient to 11.1  $\text{cm}^{-1}$  (Fig. 9c). However, addition of 5 and 10 phr NPs to this matrix increased the absorption coefficient at 0.6 THz to 12.6  $\text{cm}^{-1}$  and 13.3  $\text{cm}^{-1}$ , respectively, this time. Finally, 60 phr PSiMA monomer addition caused a steep increase in absorption coefficient at 0.6 THz to 16.6  $\text{cm}^{-1}$  as compared to 40 phr PSiMA (Fig. 9d). Similar to the PLU-20PSi, addition of 5 phr and 10 phr NPs resulted a decrease in absorption coefficient to 12.8  $\text{cm}^{-1}$  and 10.7  $\text{cm}^{-1}$ , respectively. Here we noticed that the changes in absorption coefficients appeared to be inversely correlated with the tensile strength changes. While the tensile strengths increased with the NPs addition to PLU-xPSi films, amount of decrease in absorption coefficients were appears to be correlated. For example, a significant decrease was observed for the absorption coefficient of the PLU-60PSi films from 16.6  $\text{cm}^{-1}$  to 10.7  $\text{cm}^{-1}$  while the tensile strengths were significantly increased from 3.27 to 7.54. Except PLU-40PSi films, absorption coefficient behaviors were also appeared to be correlated with the modulus behaviors. While a slight decrease in absorption was observed for PLU-20 films, a sharp decrease was observed for the PLU-60PSi films with the NPs addition. Similarly, while a slight increase was observed for the modulus of the PLU-20PSi films with the NPs addition, a sharp increase was observed for the PLU-60PSi films with the NPs addition.

Refractive indices of the polymer films were determined to be in the range of 1.5–1.73. Initially, addition of 20 phr PSiMA to PLU resulted a slight increase in the index; however, further addition resulted in a sharp decrease as observed in 40 phr PSiMA (PLU-40PSi) (Fig. 10b and c). An unexpected behavior was observed with the 60 phr addition of PSiMA to PLU where the index is recovered significantly (Fig. 10d). On the other hand, a general trend of an increase was observed with NPs addition to the UV-cured polymers. However, this trend changed to a decrease for the PLU-60PSi samples. The observed behavior appeared to be correlated with the elongation at break of the samples. The elongation at break values also decreased significantly with the addition of NPs to the PLU-60PSi system. Even though there was a drawback of change in relative amounts of

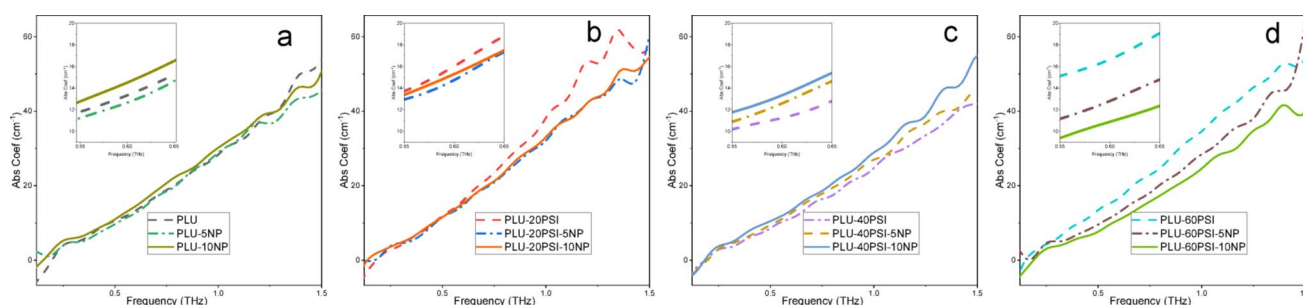


**Fig. 9** Absorption coefficient spectra of the UV-cured films

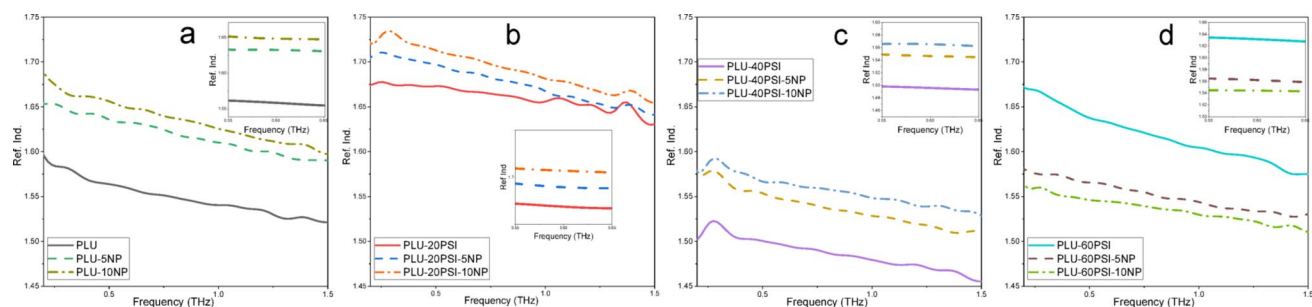


**Fig. 10** Frequency dependent refractive indices of the UV-cured films

contents with PSiMA and NPs addition, it was a very promising and significant observation that the absorption coefficient and refractive indices at THz frequencies were each correlated with certain mechanical properties of the films.

## 4 Conclusion

In this study, a novel halogen-free nanoparticle decorated UV-curable flame-retardant PLU films were developed by using phosphorous silicone methacrylate monomer (PSiMA), aliphatic urethane acrylate,  $\text{CaB}_4\text{O}_7$  nanoparticles (CBO NPs), NVP and photo-initiator. Halogen-free, flame-retardant monomer (PSiMA) was well miscible with aliphatic urethane acrylate and enhanced the flame retardancy of the PLU. This result alone suggested PSiMA monomer had a lot of promise for flame-retardant film applications. Addition of PSiMA to the structure, on the other hand, decreased the crosslink density and, thus, increased the flexibility of the film. All the mechanical properties that are affected by the PSiMA were either recovered or enhanced by the addition of the CBO NPs with its synergic effect on the film structure. Meanwhile, addition of phosphorous containing monomer lowered the degradation temperature as expected, NPs addition, once again, helped on recovering the thermal stability to the original PLU film level. This way thermal properties of the polymer films were not compromised with flame-retardant phosphorous addition in place of the halogen containing retardants. TGA results showed that PSiMA and NPs addition increased the char-formation ability to 14.5% at 750 °C under nitrogen atmosphere. The most significant improvement with the addition of PSiMA and NPs to the film structure was observed at the LOI performances. Compared to the control film (PLU, LOI = 19.5), the LOI of PLU-60PSi-10 NP increased to 27.2, an almost 40% increase in performance of the film. The main aim of this study was the improvement of flame retardancy of the PLU films without significantly compromising the thermal and mechanical properties of the PLU without the use of halogens for flame retardancy. We observed that the synergic effect between the added PSiMA monomer to the structure

and the NP addition to the film structure helped in achieving the aimed properties for the PLU films. The results showed improvement without a significant compromise for future applications of PLU film with the added effect of remarkably improved retardancy of halogen-free films.

**Supplementary Information** The online version contains supplementary material available at <https://doi.org/10.1007/s10904-025-03813-5>.

**Author Contributions** Aslı Beyler Cigil helped on development of flame-retardant NP added composite idea, responsible in the design and synthesis of the monomer and the polymer, nanoparticle inclusion, and thermal and mechanical characterization of the final composites, contributed to the data evaluation and scientific evaluations of the results, wrote most of the introduction, synthesis, characterization, and contributed to the results and discussion and conclusions. Yusuf Samet Aytekin was responsible for the THz part of the manuscript and designed the setup and measured the samples, did the data processing and evaluations, and contributed to the results and discussion and conclusions. Özde Ceren Hızal helped on development of flame-retardant NP added composite idea, was responsible for the synthesis of the nanoparticles, their x-ray and thermal characterizations, data processing, wrote the nanoparticle related parts of the manuscript, contributed to the scientific evaluations of the results, and results and discussion and conclusions. Ayşen Yılmaz oversaw the nanoparticle part of the project, contributed on characterizations and evaluations of the results, contributed on the results and discussions and the conclusions. Okan Esenturk oversaw the project, was the owner of the original idea of mixing the CBO NPs with the polymer and the flame retardants for consideration of synergic effect on better flame/fire resistance performance, contributed on system design of the THz set-up for measurements, contributed on all data evaluations, results and discussions and conclusions.

**Funding** Open access funding provided by the Scientific and Technological Research Council of Türkiye (TÜBİTAK).

**Data Availability** No datasets were generated or analysed during the current study.

## Declarations

**Competing Interests** The authors declare that they have no known competing financial interests or conflict of interest and personal relationships that could have appeared to influence the work reported in this paper.

**Open Access** This article is licensed under a Creative Commons Attribution 4.0 International License, which permits use, sharing, adaptation, distribution and reproduction in any medium or format, as long as you give appropriate credit to the original author(s) and the source, provide a link to the Creative Commons licence, and indicate if changes were made. The images or other third party material in this article are included in the article's Creative Commons licence, unless indicated otherwise in a credit line to the material. If material is not included in the article's Creative Commons licence and your intended use is not permitted by statutory regulation or exceeds the permitted use, you will need to obtain permission directly from the copyright holder. To view a copy of this licence, visit <http://creativecommons.org/licenses/by/4.0/>.

## References

- G. Phalak, D. Patil, A. Patil, S. Mhaske, Synthesis of acrylated cardanol diphenyl phosphate for UV curable flameretardant coating application. *Eur. Polym. J.* **121**, 109320 (2019)
- A. Vercasson, S. Gaucel, V. Guillard, H. Angellier-Coussy, An overview of methods to qualitatively and quantitatively characterize the structure of polymer-coated cardboards: advantages and limitations. *Mater. Des.* **252**, 113735 (2025)
- L. Huo, J. Guo, F. Yang, C. Pan, H. Hu, K. Zhang, H. Zhou, P. Liu, Design of linear polymer-based liquid lubricants by a strategy of complementary advantages. *Polymer* **265**, 125592 (2023)
- A. Agrawal, R. Kaur, Effect of nano filler on the flammability of bio-based RPUF. *Integr. Ferroelectr.* **202**, 20–28 (2019)
- G. Malucelli, Flame retardant surface treatments for rigid polyurethane foams used in the building sector: current state-of-the-art and perspectives. *Constr. Build. Mater.* **472**, 140947 (2025)
- H. Vahabi, H. Rastin, E. Movahedifar, K. Antoun, N. Brosse, M.R. Saeb, Flame retardancy of bio-based polyurethanes: opportunities and challenges. *Polymer* **12**, 1206–1234 (2020)
- H. Vahabi, R. Sonnier, L. Ferry, Effects of ageing on the fire behaviour of flameretarded polymers: a review. *Polym. Int.* **64**, 313–328 (2015)
- F. Yi, Z. Li, Q. Guo, F. Luo, J. Wu, P. Hu, Z. Liu, In situ preparation of nonflammable phosphorus-containing gel polymer electrolyte for lithium metal battery with enhanced interfacial stability and safety. *J. Chem. Eng.* **506**, 160011 (2025)
- S. Araby, B. Philips, Q. Meng, J. Ma, T. Laoui, C.H. Wang, Recent advances in carbon-based nanomaterials for flame retardant polymers and composites. *Composites B* **212**, 108675 (2021)
- Z.Z. Ma, X.W. Zhang, X.J. Zhang, N. Ahmed, H. Fan, J.T. Wan, C. Bittencourt, B.G. Li, Synthesis of CO<sub>2</sub>-derived, siloxane-functionalized poly(ether carbonate)s and waterborne polyurethanes. *Ind. Eng. Chem. Res.* **59**, 3044–3051 (2020)
- F. Tabatabaee, M. Khorasani, M. Ebrahimi, A. Gonzalez, L. Irusta, H. Sardon, Synthesis and comprehensive study on industrially relevant flame retardant waterborne polyurethanes based on phosphorus chemistry. *Prog. Org. Coat.* **131**, 397–406 (2019)
- H. Wang, X.S. Du, S. Wang, Z.L. Du, H.B. Wang, X. Cheng, Improving the flame retardancy of waterborne polyurethanes based on the synergistic effect of P-N flame retardants and a Schiff base. *RSC Adv.* **10**, 12078–12088 (2020)
- H. Liu, H. Zhang, C. Peng, S. Ren, C. Yuan, W. Luo, G. Chen, F. He, L. Dai, UV-curable waterborne polyurethane dispersions modified with a trimethoxysilane end-capping agent and edge hydroxylated Boron nitride. *J. Coat. Technol. Res.* **16**, 1479–1492 (2019)
- L. Gu, Z. Ge, M. Huang, Y. Luo, Halogen-free flame-retardant waterborne polyurethane with a novel cyclic structure of phosphorus-nitrogen synergistic flame retardant. *J. Appl. Polym. Sci.* **132**, 41288–41296 (2015)
- T. Wei, X. Zhang, Z. Shao, J. Du, H. Deng, X. Liu, Z. Lin, C. Yuan, Coregulation of crystal growth and hydroxylation induces the conversion of phosphorus-containing sludge into multifunctional hydroxyapatite nano flame retardant. *Surf. Interfaces* **60**, 106053 (2025)
- Y.C. Wang, J. Deng, J.P. Zhao, H.X. Shi, New pivot for investigating flameretarding mechanism: quantitative analysis of zinc phosphate doped aliphatic waterborne polyurethane-based intumescent coatings for flame-retarding plywood. *Polym. Adv. Technol.* **32**, 153–164 (2021)
- L. Xia, Y. Lv, Z.X. Miao, L.L. Luo, W.A. Luo, Y.T. Xu, C.H. Yuan, B.R. Zeng, L.Z. Dai, A flame retardant fabric Nanocoating based on nanocarbon black particles@polymer composite and its fire-alarm application. *Chem. Eng. J.* **433**, 11 (2022)
- B.W. Liu, H.B. Zhao, Y.Z. Wang, Advanced flame-retardant methods for polymeric materials. *Adv. Mater.* **34**, 2107905 (2022)
- L. Xia, X.H. Wang, T.T. Ren, L.L. Luo, D.X. Li, J.G. Dai, Y.T. Xu, C.H. Yuan, B.R. Zeng, L.Z. Dai, Green construction of multifunctional fire resistant epoxy resins based on boron nitride with core-shell structure. *Polym. Degrad. Stab.* **203**, 11 (2022)
- P.K. Zhang, H.J. Fan, S.Q. Tian, Y. Chen, J. Yan, Synergistic effect of phosphorus nitrogen and silicon-containing chain extenders on the mechanical properties, flame retardancy and thermal degradation behavior of waterborne polyurethane. *RSC Adv.* **6**, 72409–72422 (2016)
- L. Yan, Z.S. Xu, N. Deng, Effects of polyethylene glycol borate on the flame retardancy and smoke suppression properties of transparent fire-retardant coatings applied on wood substrates. *Prog. Org. Coat.* **135**, 123–134 (2019)
- J.D. Qiu, X.J. Lai, H.Q. Li, J.F. Gao, X.R. Zeng, X.H. Liao, Facile fabrication of a novel polyborosiloxane-decorated layered double hydroxide for remarkably reducing fire hazard of silicone rubber. *Composites B* **175**, 11 (2019)
- J. Yin, Y. Xiong, X. Zhou, Z. Yang, T. Yuan, An efficient halogen-free reactive flame-retardant active diluent for soy-castor oil-based fire safety UV-curable coatings. *Prog. Org. Coat.* **163**, 106683 (2022)
- Y. Su, S. Zhang, X. Zhou, Z. Yang, T. Yuan, A novel multi-functional bio-based reactive diluent derived from cardanol for high bio-content UV-curable coatings application. *Prog. Org. Coat.* **148**, 105880–105889 (2020)
- S. Hajirahimkhan, P.J. Ragogna, C. Xu, Methacrylation of kraft lignin for uvcurable coatings: process optimization using response surface methodology. *Biomass Bioenergy* **120**, 332–338 (2019)
- P.M. Paraskar, V.M. Hatkar, R.D. Kulkarni, Facile synthesis and characterization of renewable dimer acid-based urethane acrylate oligomer and its utilization in uvcurable coatings. *Prog. Org. Coat.* **149**, 105946–105956 (2020)
- R. Tong, L. Zhang, X. Yang, J. Liu, P. Zhou, J. Li, Emission characteristics and probabilistic health risk of volatile organic compounds from solvents in wooden furniture manufacturing. *J. Clean. Prod.* **208**, 1096–1108 (2019)
- A. Madhi, B.S. Hadavand, Bio-based UV-curable urethane acrylate graphene nanocomposites: synthesis and properties. *SN Appl. Sci.* **2**, 724 (2020)
- A. Liu, W. Tao, Y. Yang, Preparation of UV curable organic/inorganic hybrid coatings—a review. *Prog. Org. Coat.* **145**, 105685–105693 (2020)
- A. Madhi, Smart epoxy/polyurethane/carbon quantum dots hybrid coatings: synthesis and study of UV-shielding, viscoelastic, and anti-corrosive properties. *Polym. Plast. Technol. Mater.* **62**, 403–418 (2023)

31. A. Madhi, B.S. Hadavand, Tri functional biofriendly cross linker for uvcurable coatings: synthesis and study of viscoelastic properties. *Prog. Color. Color. Coat.* **14**, 199–207 (2021)
32. H. Xu, F. Qiu, Y. Wang, W. Wu, D. Yang, Q. Guo, UV-curable waterborne polyurethane-acrylate: preparation, characterization and properties. *Prog. Org. Coat.* **73**, 47–53 (2012)
33. J. Xu, Y. Jiang, F. Qiu, Y. Dai, D. Yang, Z. Yu, P. Yang, Synthesis, mechanical properties and iron surface conservation behavior of UV-curable waterborne polyurethane-acrylate coating modified with inorganic carbonate. *Polym. Bull.* **75**, 4713–4734 (2018)
34. N. Karna, P.Y. Borse, S.T. Mhaske, Advancing polyurethane acrylate coating with silane termination: influence on structural and functional performance. *Polymer* **324**, 128263 (2025)
35. X.-Y. Zhang, W.-Y. Wen, H.-Q. Yu, Q. Chen, J.-C. Xu, D.-Y. Yang, F.-X. Qiu, Preparation and artificial ageing tests in stone conservation of fluorosilicone vinyl acetate/acrylic/epoxy polymers. *Chem. Pap.* **70**, 1621–1631 (2016)
36. Q. Chen, W.-Y. Wen, F.-X. Qiu, J.-C. Xu, H.-Q. Yu, M.-L. Chen, D.-Y. Yang, Preparation and application of modified carboxymethyl cellulose si/polyacrylate protective coating material for paper relics. *Chem. Pap.* **70**, 946–959 (2016)
37. L. Wan, L.C. Deng, H. Chen, Z.-Y. Zhao, S.-C. Huang, W.-C. Wei, A.-H. Yang, H.-B. Zhao, Y.-Z. Wang, Flame retardant thermoplastic polyurethane elastomer: from organic materials to nanocomposites and new prospects. *Chem. Eng. J.* **417**, 129314 (2021)
38. L.H. Pham, N.T. Nguyen, D.M. Nguyen, T.A. Nguyen, T.B. Nguyen, J. Suhr, T.D. Nguyen, M. Rahim, A.D. Tran-Le, L. Terrei, R. Mehaddi, Y.F. da Silva, P. Perré, D.Q. Hoang, Effective non-halogen flame-retardants combined with nSiO<sub>2</sub> particles to improve thermal stability and fire resistance of high-performance polyurethane nanocomposite foams. *J. Mater. Sci.* **203**, 1–13 (2024)
39. M. Dogan, S.D. Dogan, L.A. Savas, C. Ozcelik, U. Tayfun, Flame retardant effect of boron compounds in polymeric materials. *Composites B* **222**, 1090888 (2021)
40. T. Zhang, S. Huo, G. Ye, C. Wang, Q. Zhang, Y. Xue, P. Song, H. Wang, Z. Liu, Phosphorus/boron-containing, flame-retardant polyurethane elastomers with great mechanical, shape-memory, and recycling performances. *Polym. Degrad. Stab.* **230**, 111047 (2024)
41. S.R. Acharya, S. Mohanty, A.K. Palai, Flame retardant rigid polyurethane foam derived from biobased polyols and water as Co-blowing agent: synergistic effect of expanded graphite and boron nitride. *Mater. Today Commun.* **41**, 110278 (2024)
42. G. Ozcelik, O. Elcin, S. Guney, A. Erdem, F. Hacioglu, M. Dogan, Flame-retardant features of various boron compounds in thermoplastic polyurethane and performance comparison with aluminum trihydroxide and magnesium hydroxide. *Fire Mater.* **46**, 1020–1033 (2022)
43. K. Kim, M. Kim, J. Kim, Fabrication of UV-curable polyurethane acrylate composites containing surface-modified boron nitride for underwater sonar encapsulant application. *Ceram. Int.* **40**, 10933–10943 (2014)
44. Y. Ma, H. Huang, S. Hao, K. Qiu, H. Gao, L. Gao, Insights into the water status in hydrous minerals using terahertz time-domain spectroscopy. *Sci. Rep.* **9**, 2665 (2019)
45. M. Manjappa, R. Singh, Materials for terahertz optical science and technology. *Adv. Opt. Mater.* **8**, 1901984 (2020)
46. F. D'Angelo, Z. Mics, M. Bonn, D. Turchinovich, Ultra-broadband THz time-domain spectroscopy of common polymers using THz air photonics. *Opt. Express* **22**, 12475 (2014)
47. T. Kleine-Ostmann, T. Nagatsuma, A review on terahertz communications research. *J. Infrared Millim. Terahertz Waves* **32**, 143–171 (2011)
48. M.D. King, P.M. Hakey, T.M. Korter, Discrimination of chiral solids: a terahertz spectroscopic investigation of L- and DL-serine. *J. Phys. Chem. A* **114**, 2945–2953 (2010)
49. H. Feng, D. An, H. Tu, W. Bu, W. Wang, Y. Zhang, H. Zhang, X. Meng, W. Wei, B. Gao, S. Wu, A passive video-rate terahertz human body imager with real-time calibration for security applications. *Appl. Phys. B* **126**, 143 (2020)
50. O. Peters, S.F. Busch, B.M. Fischer, M. Koch, Determination of the carbon nanotube concentration and homogeneity in resin films by THz spectroscopy and imaging. *J. Infrared Millim. Terahertz Waves* **33**, 1221–1226 (2012)
51. R. Casini, G. Papari, A. Andreone, D. Marrazzo, A. Patti, P. Russo, Dispersion of carbon nanotubes in melt compounded polypropylene based composites investigated by THz spectroscopy. *Opt. Express* **23**, 18181 (2015)
52. Y. Ji, Y.Y. Huang, R. Rungsawang, E.M. Terentjev, Dispersion and alignment of carbon nanotubes in liquid crystalline polymers and elastomers. *Adv. Mater.* **22**, 3436–3440 (2010)
53. S. Kumar, N. Kamaraju, B. Karthikeyan, M. Tondusson, E. Freysz, A.K. Sood, Terahertz spectroscopy of Single-Walled carbon nanotubes in a polymer film: observation of low-frequency phonons. *J. Phys. Chem. C* **114**, 12446–12450 (2010)
54. R. Rungsawang, V.G. Geethamma, E.P.J. Parrott, D.A. Ritchie, E.M. Terentjev, Terahertz spectroscopy of carbon nanotubes embedded in a deformable rubber. *J. Appl. Phys.* **103**, 123503 (2008)
55. F. Destic, C. Bouvet, Impact damages detection on composite materials by THz imaging. *Case Stud. Nondestruct. Test. Eval.* **6**, 53–62 (2016)
56. A. Beyler-Çiğil, M.V. Kahraman, Effect of surface modification on nano-diamond particles for surface and thermal property of UV-curable hybrid coating. *Prog. Org. Coat.* **101**, 468–476 (2016)
57. Y.S. Aytakin, M. Köktürk, A. Zaczek, T.M. Korter, E.J. Heilweil, O. Esenturk, Optical properties of meloxicam in the far-infrared-spectral region. *Chem. Phys.* **512**, 36–43 (2018)
58. Y. Jiang, P. Yan, Y. Wang, C. Zhou, J. Lei, Form-stable phase change materials with enhanced thermal stability and fire resistance via the incorporation of phosphorus and silicon. *Mater. Des.* **160**, 763–771 (2018)
59. F. Dodangeh, M.S. Seyed Dorraji, M.H. Rasoulifard, H.R. Ashjari, Synthesis and characterization of alkoxy silane modified polyurethane wood adhesive based on epoxidized soybean oil polyester polyol. *Composites B* **187**, 107857–107894 (2020)
60. H. Abdollahi, V. Najafi, F. Amiri, Determination of monomer reactivity ratios and thermal properties of poly(GMA-co-MMA) copolymers. *Polym. Bull.* **78**, 493–511 (2021)
61. A. Darvishia, M.J.Z. Mehrb, G.B. Marandia, K. Kabirib, H. Bouhendi, H. Bakhshi, Copolymers of glycidyl methacrylate and octadecyl acrylate: synthesis, characterization, swelling properties, and reactivity ratios. *Des. Monomers Polym.* **16**, 79–88 (2013)
62. B.J. Saikia, S.K. Dolui, Designing semiencapsulation based covalently self-healable poly(methyl methacrylate) composites by atom transfer radical polymerization. *J. Polym. Sci. Polym. Chem.* **54**, 1842–1851 (2016)
63. L. Feng, W. Wang, B. Song, X. Zhu, L. Wang, R. Shao, T. Li, X. Pei, L. Wang, X. Qian, Z. Xu, Synthesis of P, N and Si-containing waterborne polyurethane with excellent flame retardant, alkali resistance and flexibility via one-step synthetic approach. *Prog. Org. Coat.* **174**, 107286 (2023)
64. S. Solgi, M.J. Tafreshi, M.S. Ghamsari, A facile route for synthesis of highly pure  $\alpha$ -CaB<sub>4</sub>O<sub>7</sub> compound. *Mater. Res. Express* **6**, 026205 (2019)
65. E. Cakmakçı, Allylamino diphenylphosphine oxide and poss containing flame retardant photocured hybrid coatings. *Prog. Org. Coat.* **105**, 37–47 (2017)

66. P. Zheng, R. Wang, D. Wang, X. Peng, Y. Zhao, Q. Liu, A phosphorus-containing hyperbranched phthalocyanine flame retardant for epoxy resins. *Sci. Rep.* **11**, 1–10 (2021)
67. Y. Chen, L. Li, L. Qian, The pyrolysis behaviors of phosphorus-containing organosilicon compound modified ammonium polyphosphate with different phosphorus-containing groups, and their different flame-retardant mechanisms in polyurethane foam. *RSC Adv.* **8**, 27470–27480 (2018)
68. S.-C. Wang, P.-C. Chen, C.-J. Peng, J.-Z. Hwang, K.-N. Chen, Flame retardation behaviors of UV-curable phosphorus-containing PU coating system. *J. Polym. Eng.* **33**, 749–756 (2013)
69. G. Sagdic, E. Cakmakci, O. Daglar, U.S. Gunay, G. Hizal, U. Tunca, H. Durmaz, Thermal and mechanical properties of thiol-ene photocured thermosets containing DOPO-based liquid reactive flame retardant synthesized by metal-free azide-alkyne click reaction. *Prog. Org. Coat.* **167**, 106825 (2022)
70. Y.L. Xing, Y.Q. Li, Z.J. Lin, X. Ma, H. Qu, R.L. Fan, Synthesis and characterization of bio-based intumescent flame retardant and its application in polyurethane. *Fire Mater.* **44**, 814–824 (2020)
71. X. Yin, H.S. Pang, Y.J. Luo, B. Zhang, Eco-friendly functional two-component flame-retardant waterborne polyurethane coatings: a review. *Polym. Chem.* **12**, 5400–5411 (2021)
72. A. Beyler-Çiğil, Designing superhydrophobic and flame retardant photo-cured hybrid coatings. *Prog. Org. Coat.* **148**, 105850 (2020)
73. O. Daglar, E. Çakmakçi, U.S. Gunay, G. Hizal, U. Tunca, H. Durmaz, Acetylene dicarboxylic acid diallyl ester: a versatile monomer for thiol-ene photocured networks. *Macromol. Mater. Eng.* **306**, 2100427 (2021)
74. A. Madhi, Green fluorescent unsaturated polyester/graphitic carbon nitride quantum dots nanocomposites: preparation and study of UV-resistance, mechanical and viscoelastic properties. *J. Compos. Mater.* **57**, 2437–2450 (2023)

**Publisher's Note** Springer Nature remains neutral with regard to jurisdictional claims in published maps and institutional affiliations.